Supporting Information for

A Molecular Strategy for Raman Enhancement

Ying-Fan Tan[1]†, Yangbo Zhang[1]†, Xiong Wang[2], Ning Zhou[1], Qingyun Wan[1]*

[1]Department of Chemistry, The Chinese University of Hong Kong, Hong Kong, China.

[2]Department of Physics, The University of Hong Kong, Pokfulam Road, Hong Kong, China.

*Corresponding author: qingyunwan@cuhk.edu.hk

†These authors contributed equally to this work.

Table of Content

1. Experimental Section

The following materials were used as received:

Tetrabutylammonium bis(1,3-dithiole-2-thione-4,5-dithiolato)nickel(III) and bis(tetrabutylammonium) bis(1,3-dithiole-2-thione-4,5-dithiolato)palladium(II) (TCI) Bis(tetrabutylammonium) bis(1,3-dithiole-2-thione-4,5-dithiolato)zinc, rhodamine 6G, and rhodamine 19 perchlorate (Macklin).

Solvents: Acetonitrile (ACS grade), methanol (ACS grade), ethanol (ACS grade), diethyl ether (2000 ppm water, stabilized with BHT, ACS grade), and dichloromethane (HPLC grade) (RCI Labscan, Thailand). *n*-Hexane (95%, ACS grade, Duksan, Korea). DMSO-d_6 (J&K Scientific). Deionized water was obtained using a Thermo Scientific Smart2Pure 6 UV purification system.

Ni-1: ^{1}H-NMR (500 MHz, DMSO-d_6) δ 8.13 (br, 1H), 7.83 (br, 1H), 7.77 (br, 1H), 7.36 (br, 1H), 6.66 (s, 2H), 6.59 (s, 2H), 3.46 – 3.39 (m, 4H), 2.07 (s, 6H), 1.25 (br, 6H).

Pd-1: ^{1}H-NMR (500 MHz, DMSO-d_6) δ 13.01 (s, 1H), 8.21 (d, J = 8.2 Hz, 1H), 7.85 (t, J = 7.5 Hz, 1H), 7.79 (t, J = 7.6 Hz, 1H), 7.60 (br, 2H), 7.40 (d, J = 7.8 Hz, 1H), 6.88 (s, 2H), 6.76 (s, 2H), 3.49 – 3.44 (m, 4H), 2.08 (s, 6H), 1.25 (t, J = 7.1 Hz, 6H).

Zn-1: ^{1}H-NMR (500 MHz, DMSO-d_6) δ 13.02 (s, 1H), 8.20 (br, 1H), 7.85 (t, J = 7.6 Hz, 1H), 7.79 (t, J = 7.5 Hz, 1H), 7.65 (br, 2H), 7.40 (d, J = 5.8 Hz, 1H), 6.87 (s, 2H), 6.76 (s, 2H), 3.45 (br, 4H), 3.18 – 3.14 (m, 8H), 2.07 (s, 6H), 1.57 (p, J = 8.0 Hz, 8H), 1.35 – 1.28 (m, 8H), 1.25 (t, J = 7.1 Hz, 6H), 0.93 (t, J = 7.3 Hz, 12H).

Ni-2: ^{1}H-NMR (500 MHz, DMSO-d_6) δ 8.23 (d, J = 7.3 Hz, 1H), 7.93 (br, 1H), 7.86 (br, 1H), 7.60 (br, 3H), 6.86 (s, 2H), 6.79 (s, 2H), 3.94 (br, 2H), 3.59 (br, 4H), 2.19 (s, 6H), 1.29 (br, 6H), 0.84 (t, J = 6.5 Hz, 3H).

Pd-2: ^{1}H-NMR (500 MHz, DMSO-d_6) δ 8.24 (d, J = 7.8 Hz, 1H), 7.90 (t, J = 7.4 Hz, 1H), 7.83 (t, J = 7.7 Hz, 1H), 7.70 (t, J = 6.0 Hz, 2H), 7.47 (d, J = 7.5 Hz, 1H), 6.94 (s, 2H), 6.80 (s, 2H), 3.94 (q, J = 7.1 Hz, 2H), 3.49 (p, J = 7.2 Hz, 4H),

2.09 (s, 6H), 1.26 (t, *J* = 7.1 Hz, 6H), 0.84 (t, *J* = 7.1 Hz, 3H).

Zn-2: ^{1}H-NMR (500 MHz, DMSO-d_6) δ 8.24 (d, *J* = 7.9 Hz, 1H), 7.90 (t, *J* = 7.5 Hz, 1H), 7.83 (t, *J* = 7.7 Hz, 1H), 7.70 (br, 2H), 7.47 (d, *J* = 7.6 Hz, 1H), 6.94 (s, 2H), 6.80 (s, 2H), 3.94 (q, *J* = 7.2 Hz, 2H), 3.51 – 3.47 (m, 4H), 3.19 – 3.13 (m, 8H), 2.09 (s, 6H), 1.57 (p, *J* = 7.9 Hz, 8H), 1.35 – 1.28 (m, 8H), 1.26 (t, *J* = 7.2 Hz, 6H), 0.93 (t, *J* = 7.3 Hz, 12H), 0.84 (t, *J* = 7.1 Hz, 3H).

[Ni]: A solution of tetrabutylammonium bis(1,3-dithiole-2-thione-4,5-dithiolato)nickel(III) (4 mg) in acetonitrile (2 mL) was subjected to vapor diffusion of diethyl ether, yielding elongated green crystals (1.7 mg, yield: 43%).

[Pd]: Commercially obtained bis(tetrabutylammonium) bis(1,3-dithiole-2-thione-4,5-dithiolato)palladium(II) (purple needle-like crystals) was used directly for Raman spectroscopy.

[Zn]: A solution of bis(1,3-dithiole-2-thione-4,5-dithiolato)zinc (5 mg) in dichloromethane (1 mL) was layered with hexane (1 mL). After 12 h, red plate crystals formed (2.6 mg, yield: 52%).

1: A solution of rhodamine 19 perchlorate (2 mg) in acetonitrile (0.7 mL) was subjected to vapor diffusion of diethyl ether, yielding red crystals after 12 h (0.7 mg, yield: 35%).

^{1}H-NMR (500 MHz, DMSO-d_6) δ 13.03 (s, 1H), 8.23 (d, *J* = 7.9 Hz, 1H), 7.86 (t, *J* = 7.5 Hz, 1H), 7.80 (t, *J* = 7.6 Hz, 1H), 7.68 (br, 2H), 7.42 (d, *J* = 7.5 Hz, 1H), 6.92 (s, 2H), 6.80 (s, 2H), 3.48 (p, *J* = 7.1 Hz, 4H), 2.09 (s, 6H), 1.26 (t, *J* = 7.2 Hz, 6H).

2: A solution of rhodamine 6G (7 mg) in dichloromethane (2 mL) was layered with hexane (1 mL). After several days, red plate crystals formed (4 mg, yield: 57%).

^{1}H-NMR (500 MHz, DMSO-d_6) δ 8.24 (d, *J* = 7.8 Hz, 1H), 7.90 (t, *J* = 7.6 Hz, 1H), 7.83 (t, *J* = 7.6 Hz, 1H), 7.75 (t, *J* = 6.0 Hz, 2H), 7.47 (d, *J* = 7.6 Hz, 1H), 6.94 (s, 2H), 6.80 (s, 2H), 3.94 (q, *J* = 7.0 Hz, 2H), 3.49 (p, *J* = 7.2 Hz, 4H), 2.10 (s, 6H), 1.26 (t, *J* = 7.2 Hz, 6H), 0.84 (t, *J* = 7.1 Hz, 3H).

All the crystals powder were collected by filtration, washed with diethyl ether and dried in vacuum for further characterization and measurement.

2. Raman Spectra

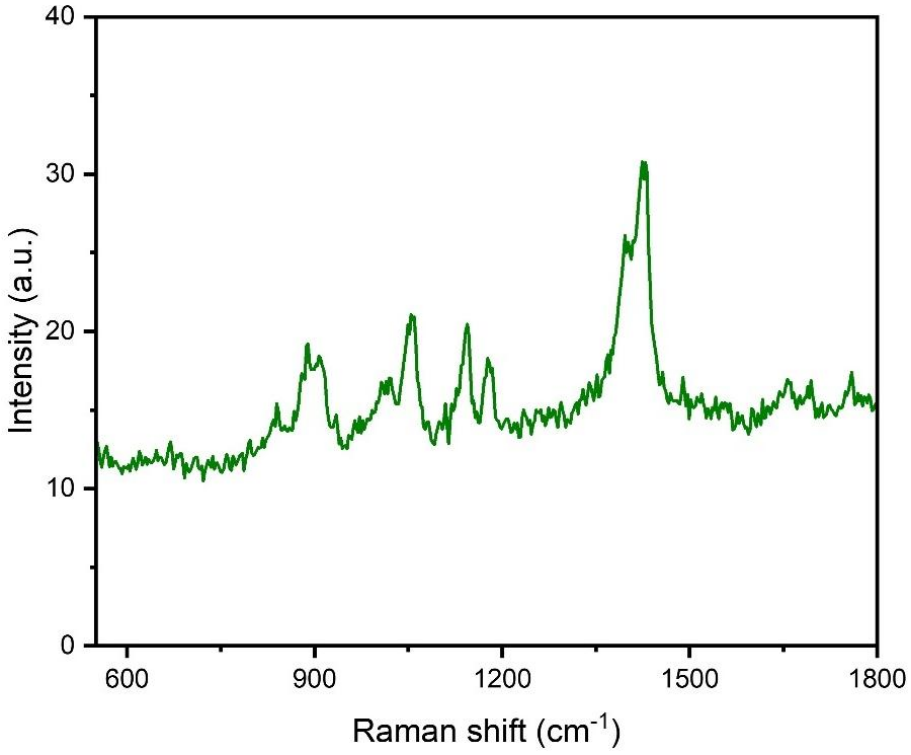

Figure S1. Raman spectrum of [**Ni**] single crystal (λ_{ex} = 532 nm).

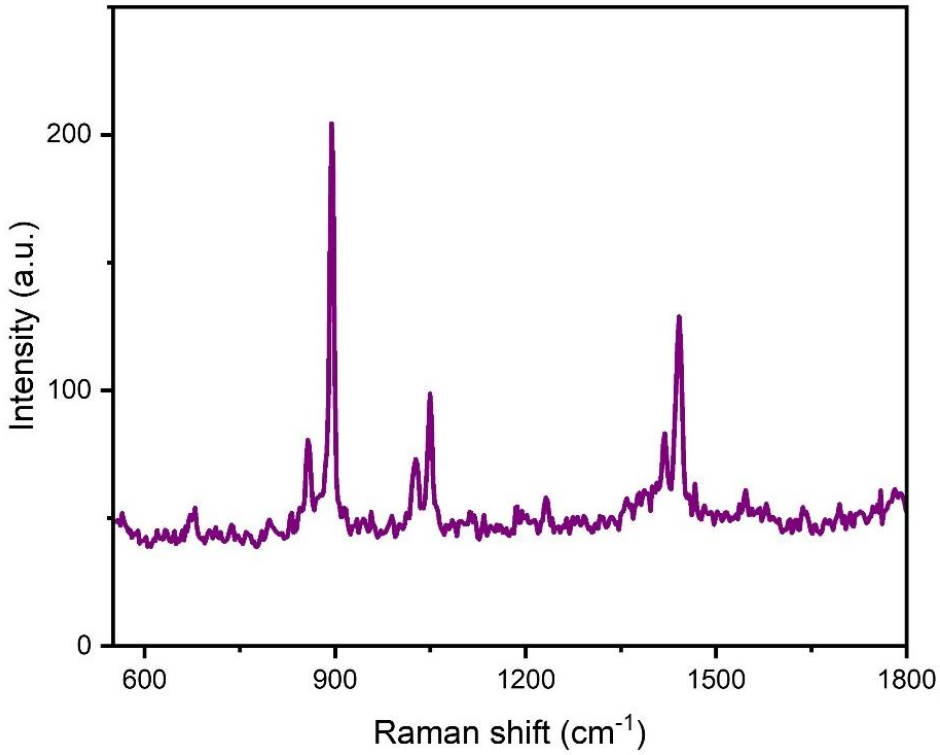

Figure S2. Raman spectrum of [**Pd**] single crystal (λ_{ex} = 532 nm).

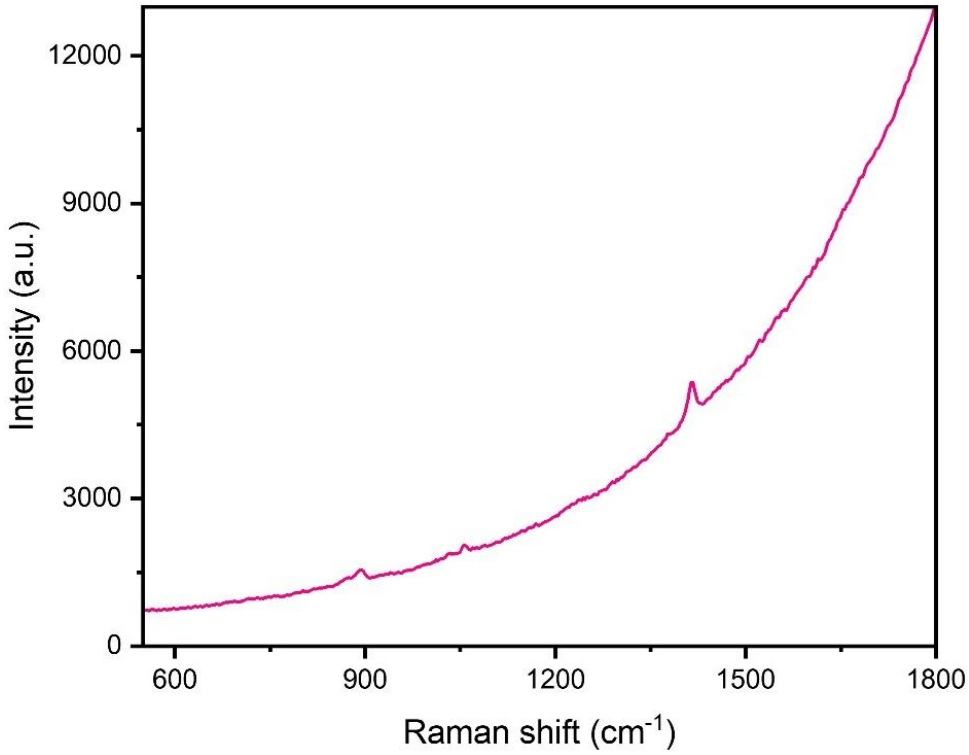

Figure S3. Raman spectrum of [**Zn**] single crystal (λ_{ex} = 532 nm).

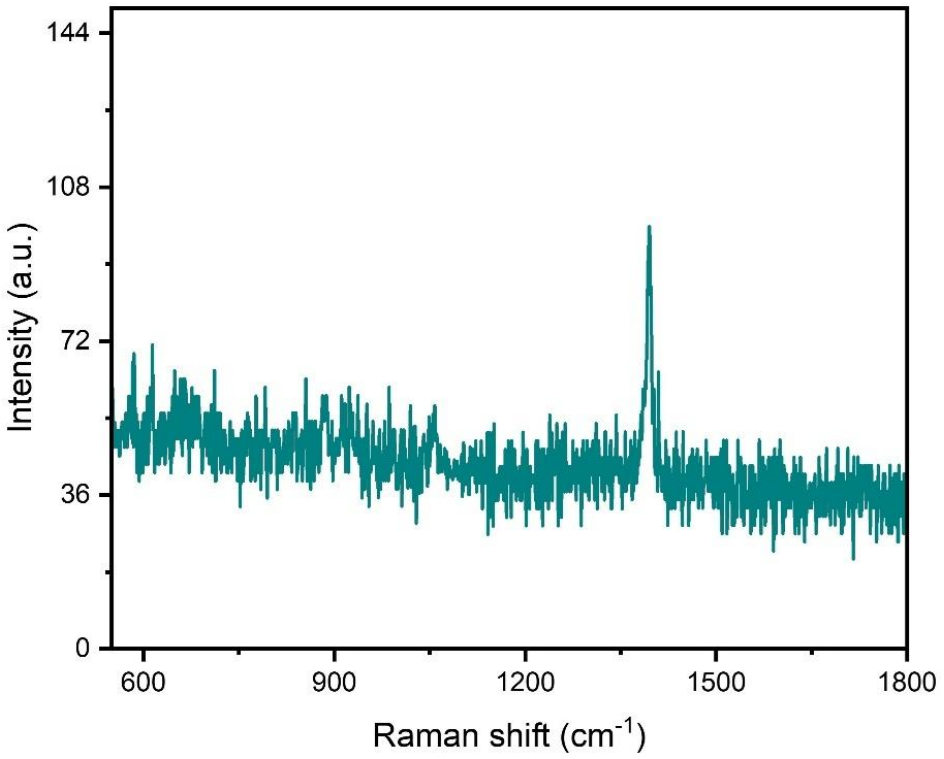

Figure S4. Raman spectrum of **Ni-2** single crystal with 785 nm excitation wavelength.

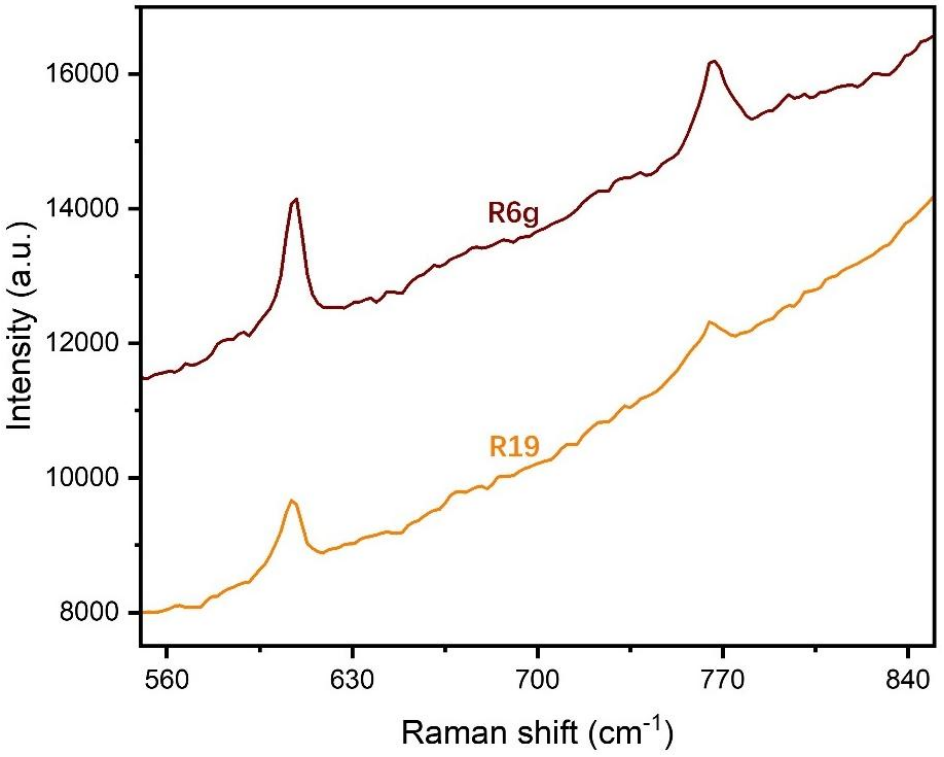

Figure S5. Averaged Raman spectrum of **R6g** and **R19** dried from their respective solution with concentration = 1×10^{-3} M.

*Raw data of **R19/R6g+[M]** at specific concentrations*

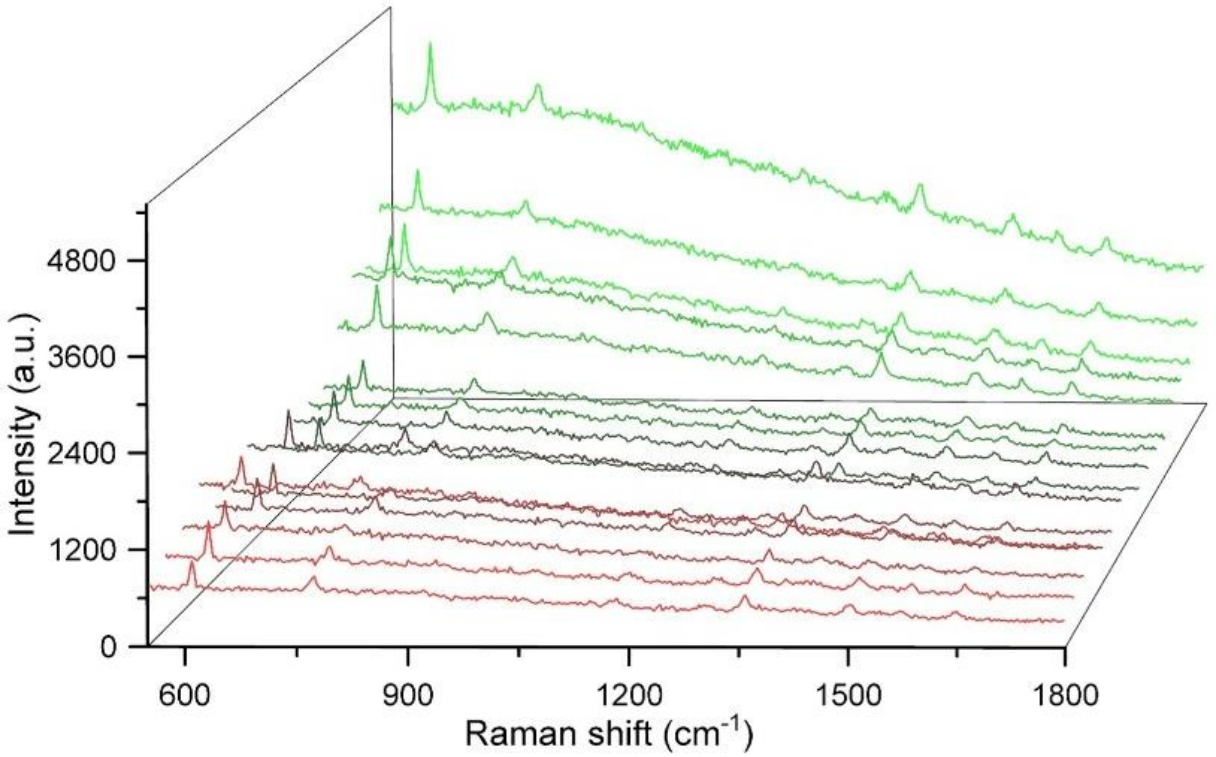

Figure S6. Raman spectra of dried mixed solution: [**R19**] = 1×10^{-6} M + [**Ni**] = 5×10^{-5} M (λ_{ex} = 532 nm).

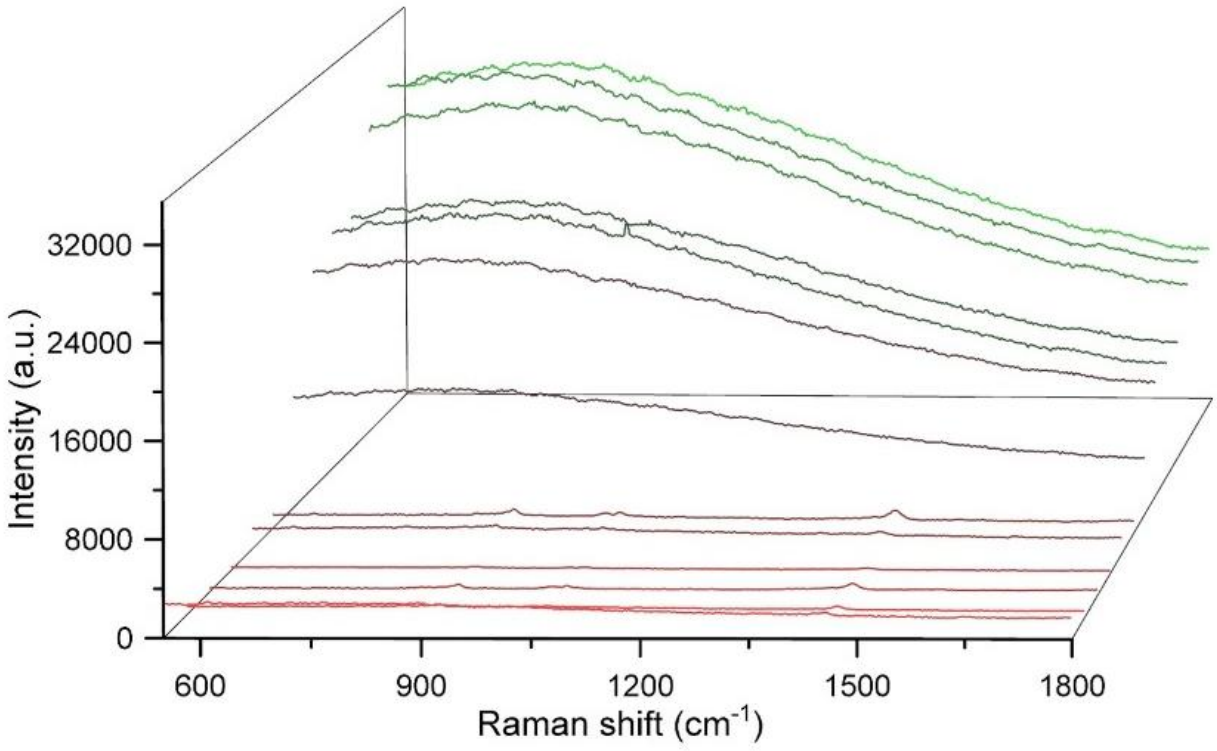

Figure S7. Raman spectra of dried mixed solution: [**R19**] = 1×10^{-6} M + [**Pd**] = 5×10^{-5} M (λ_{ex} = 532 nm).

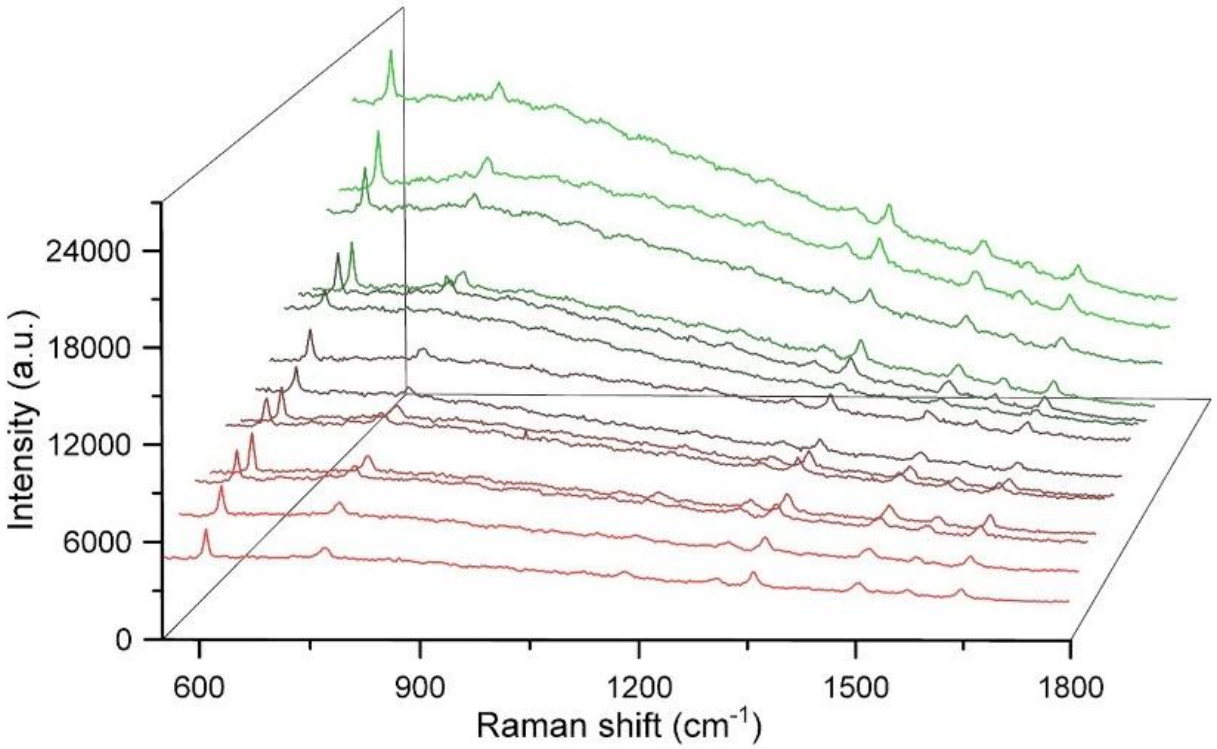

Figure S8. Raman spectra of dried mixed solution: [**R19**] = 1×10^{-6} M + [**Ni**] = 1×10^{-5} M (λ_{ex} = 532 nm).

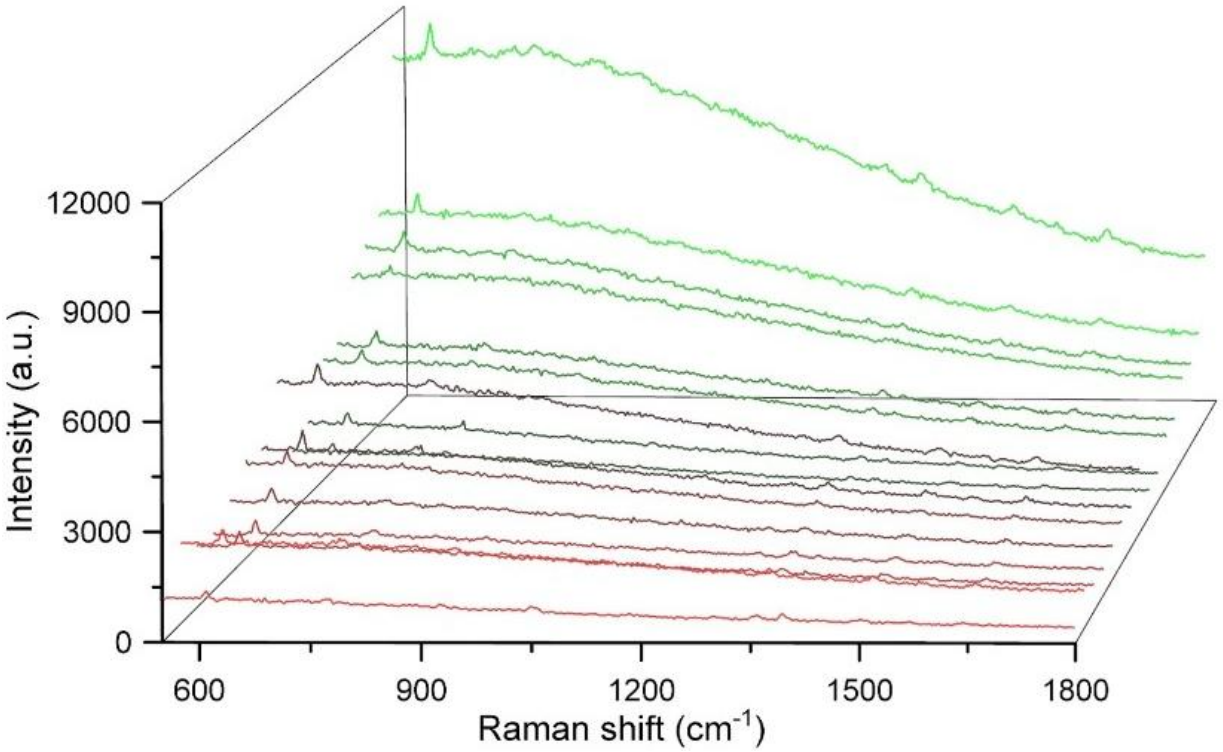

Figure S9. Raman spectra of dried mixed solution: [**R19**] = 1×10^{-6} M + [**Ni**] = 1×10^{-4} M (λ_{ex} = 532 nm).

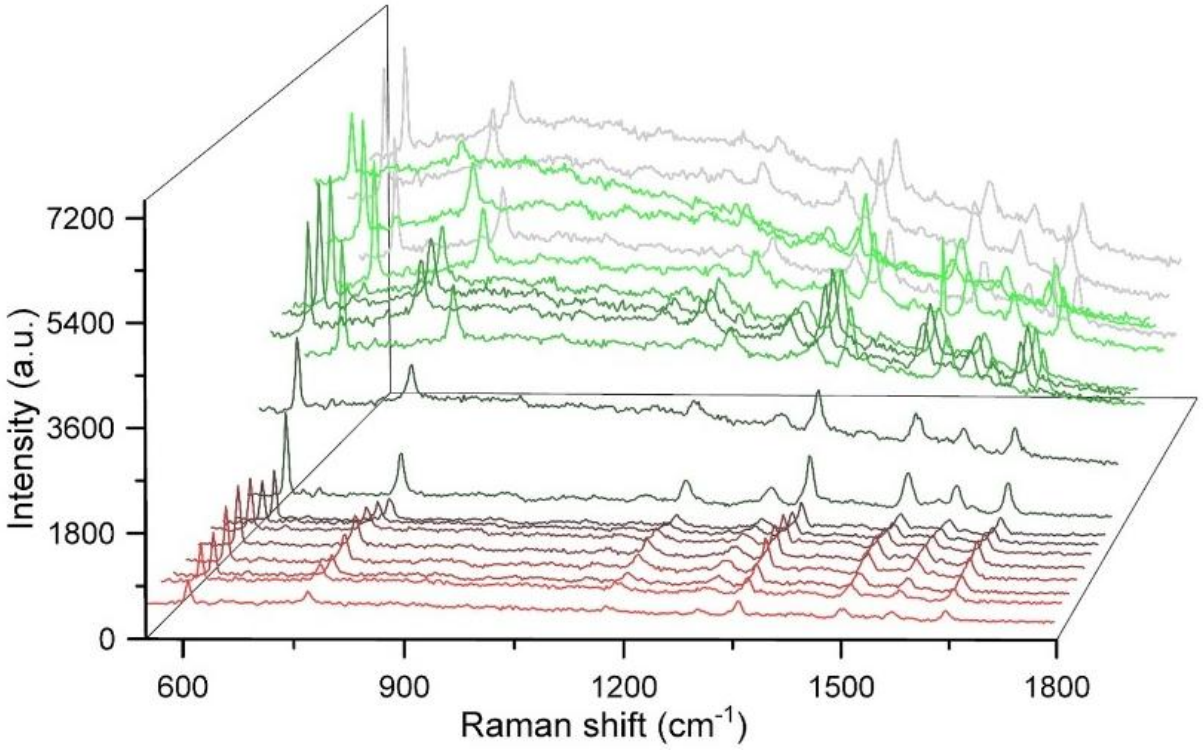

Figure S10. Raman spectra of dried mixed solution: [**R6g**] = 1×10^{-6} M + [**Ni**] = 5×10^{-5} M (λ_{ex} = 532 nm).

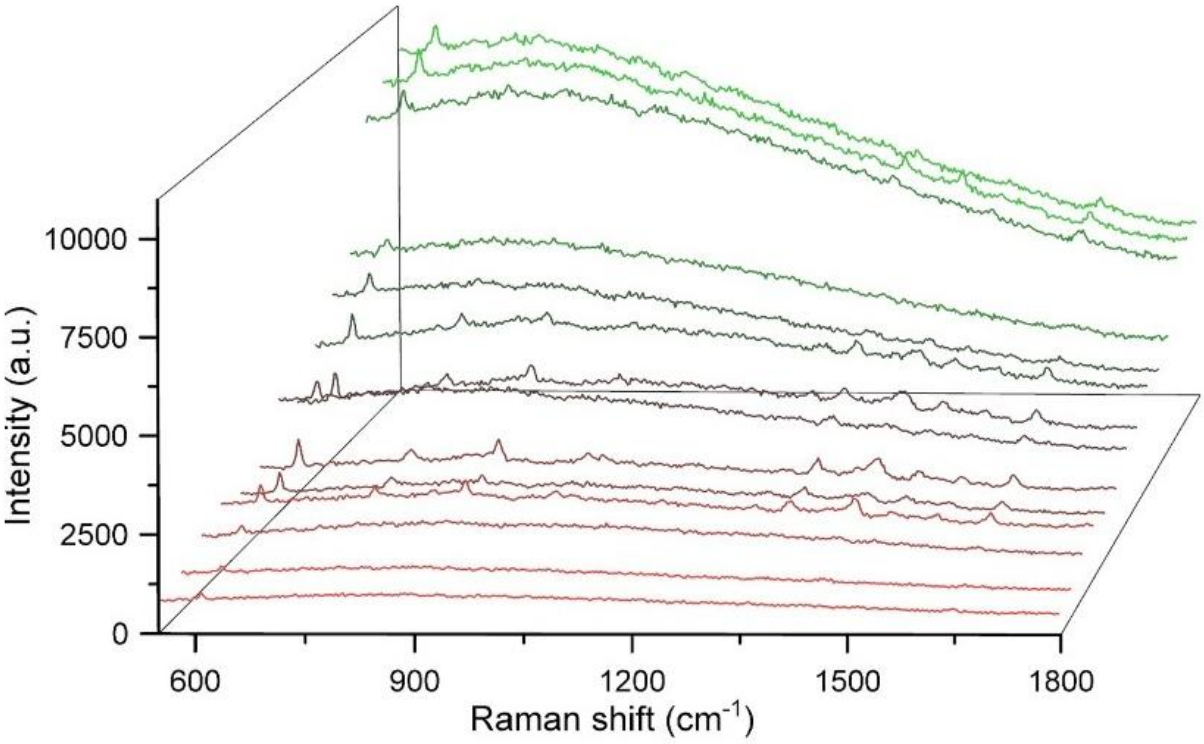

Figure S11. Raman spectra of dried mixed solution: [**R6g**] = 1×10^{-6} M + [**Pd**] = 5×10^{-5} M (λ_{ex} = 532 nm).

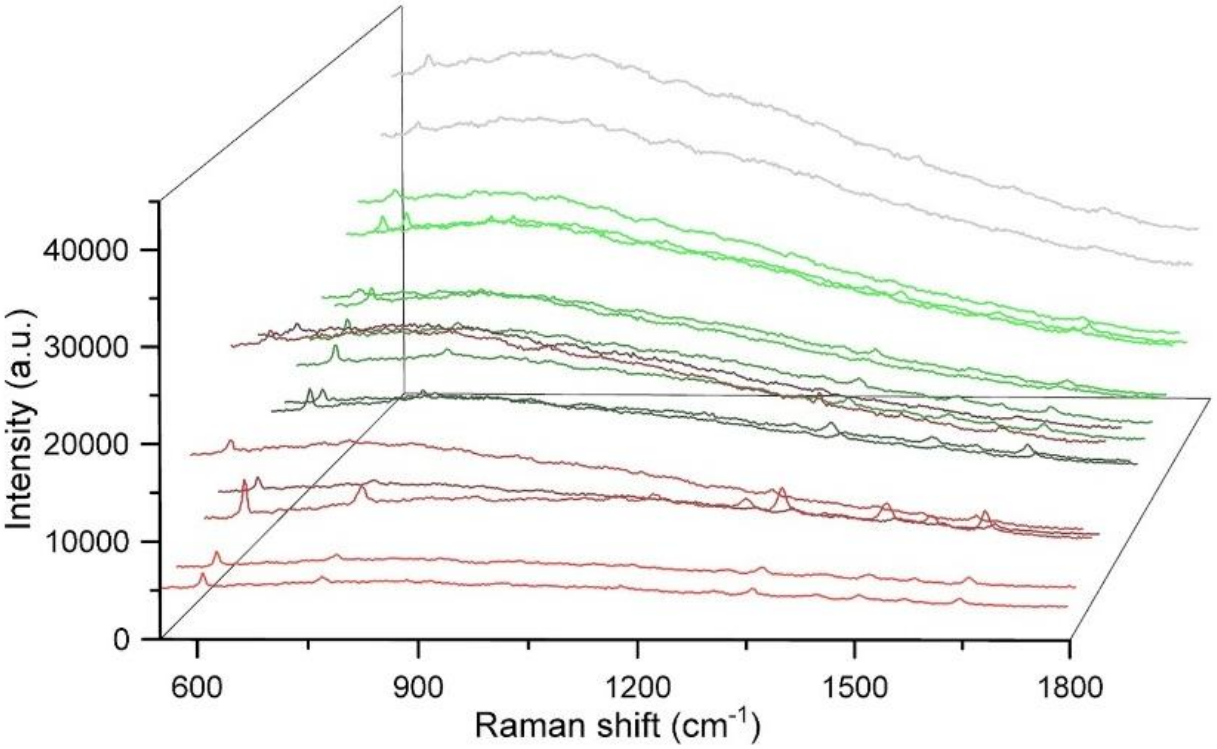

Figure S12. Raman spectra of dried mixed solution: [**R6g**] = 1×10^{-6} M + [**Ni**] = 1×10^{-5} M (λ_{ex} = 532 nm).

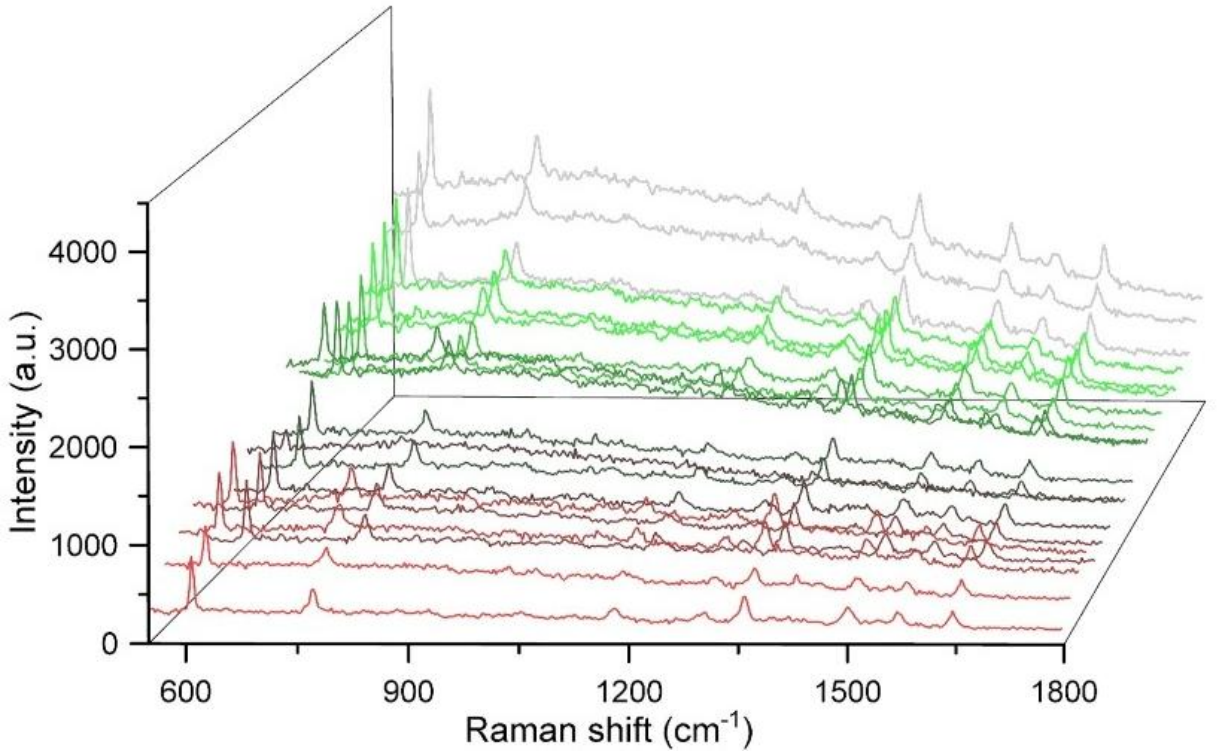

Figure S13. Raman spectra of dried mixed solution: [**R6g**] = 1×10^{-6} M + [**Ni**] = 1×10^{-4} M (λ_{ex} = 532 nm).

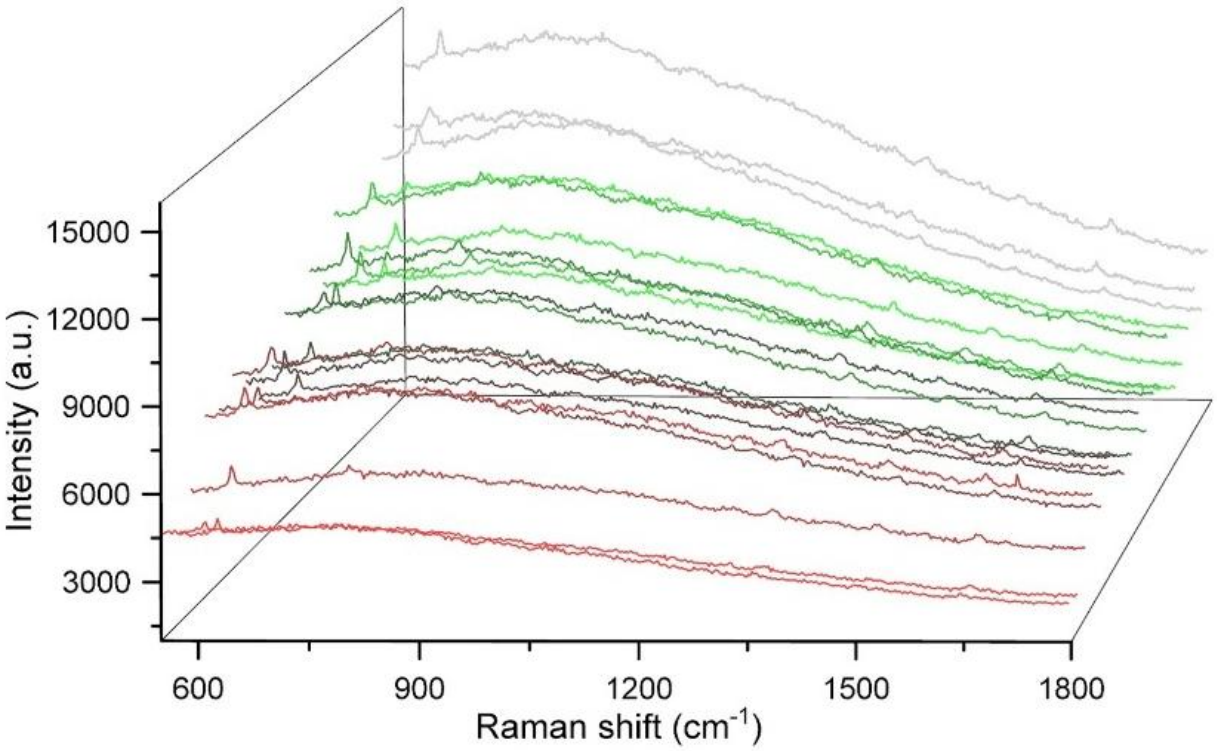

Figure S14. Raman spectra of dried mixed solution: [**R6g**] = 1×10^{-7} M + [**Ni**] = 1×10^{-5} M (λ_{ex} = 532 nm).

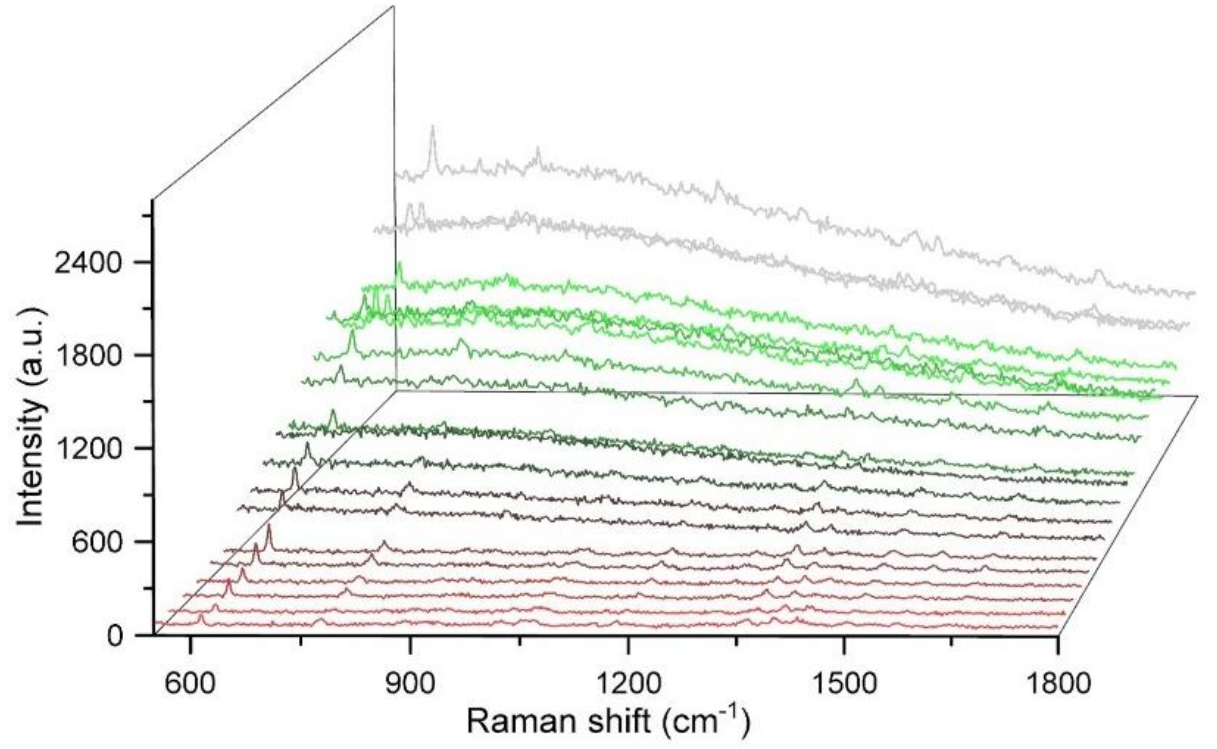

Figure S15. Raman spectra of dried mixed solution: [**R6g**] = 1×10^{-8} M + [**Ni**] = 1×10^{-5} M (λ_{ex} = 532 nm).

3. EF (Enhanced Factor)

The EF was calculated according to the following formula[1, 2]:

$$EF = \frac{(\frac{I_{SERS}}{N_{SERS}})}{(\frac{I_{reference}}{N_{reference}})} \quad (1)$$

$$N_{SERS}\ or\ N_{reference} = CVN_A \frac{A_{Raman}}{A_{sub}} \quad (2)$$

Here, I_{SERS} and $I_{reference}$ represent enhanced and normal Raman intensities, while N_{SERS} and $N_{reference}$ denote the number of **R19**/**R6G** molecules contributing to these signals. For analyte molecules on Si/SiO_2 wafers, N values were estimated assuming uniform distribution, where C is molar concentration (SERS: 1×10^{-6} M **R19**/**R6G** + 5×10^{-5} M [**Ni**]/[**Pd**]; reference: 1×10^{-3} M **R19**/**R6G**), V is droplet volume (5 μL), N_A is Avogadro's constant, A_{Raman} is laser spot area (44.2 μm^2), and A_{sub} is effective substrate area (~3 mm diameter from evaporated droplet).

Table S1. EF of **R19**/**R6G**, accounting for CT effects.

Probe Molecule	CT complex	EF
R19	**[Ni]**	475.1
R19	**[Pd]**	130.5
R6g	**[Ni]**	860.8
R6g	**[Pd]**	336.8

4. Reflectance Spectra

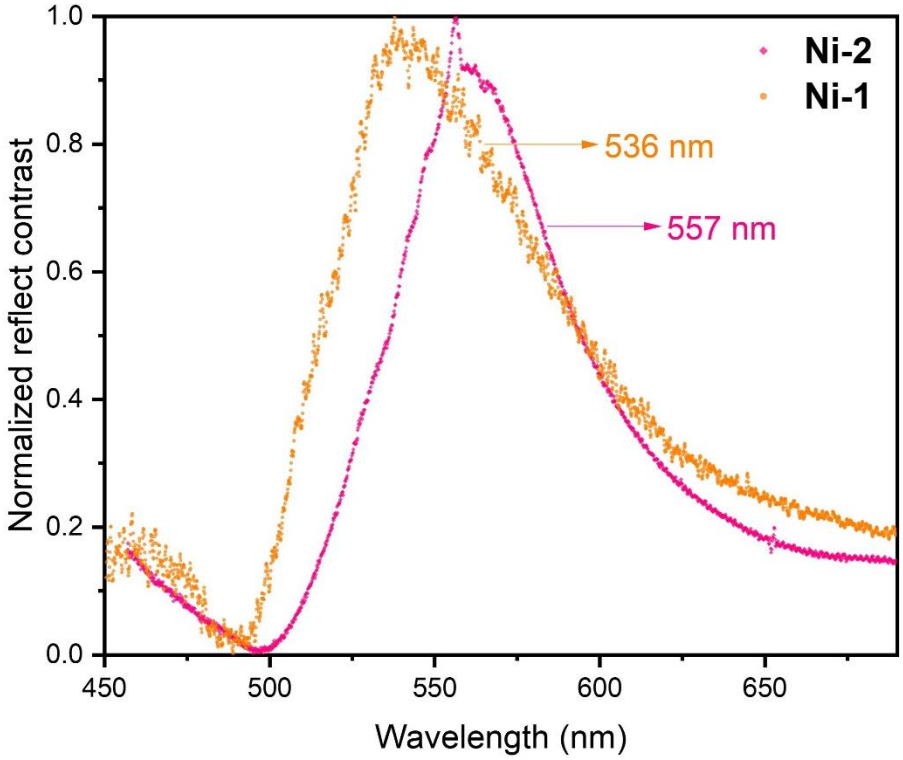

Figure S16. Reflectance spectra of **Ni-1/2** single crystals

5. UV-vis Spectra

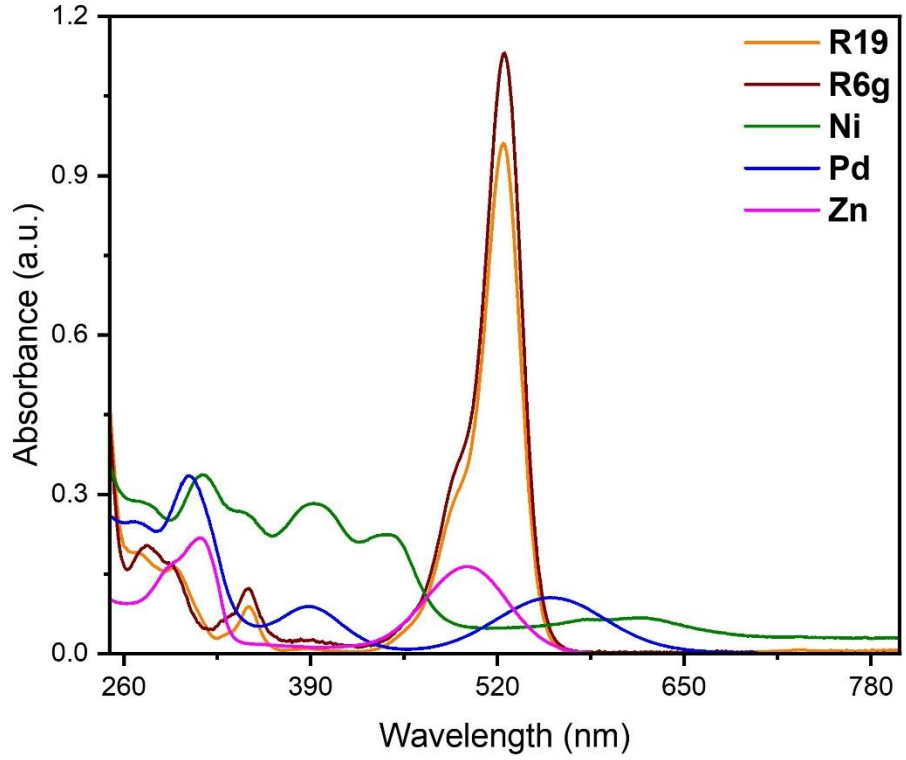

Figure S17. UV-vis spectra in acetonitrile at a concentration of 1×10^{-5} M.

6. ^{1}H-NMR Spectra

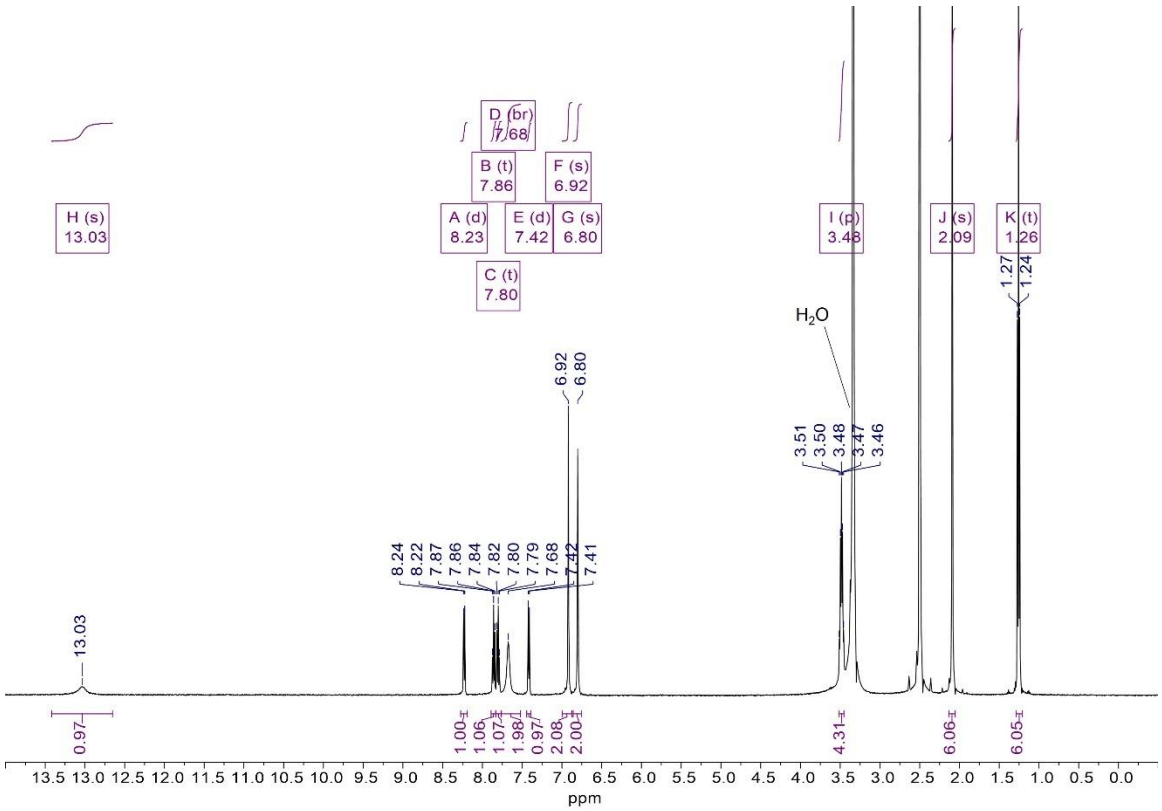

Figure S18. ^{1}H-NMR spectra of **R19** in DMSO-d_6

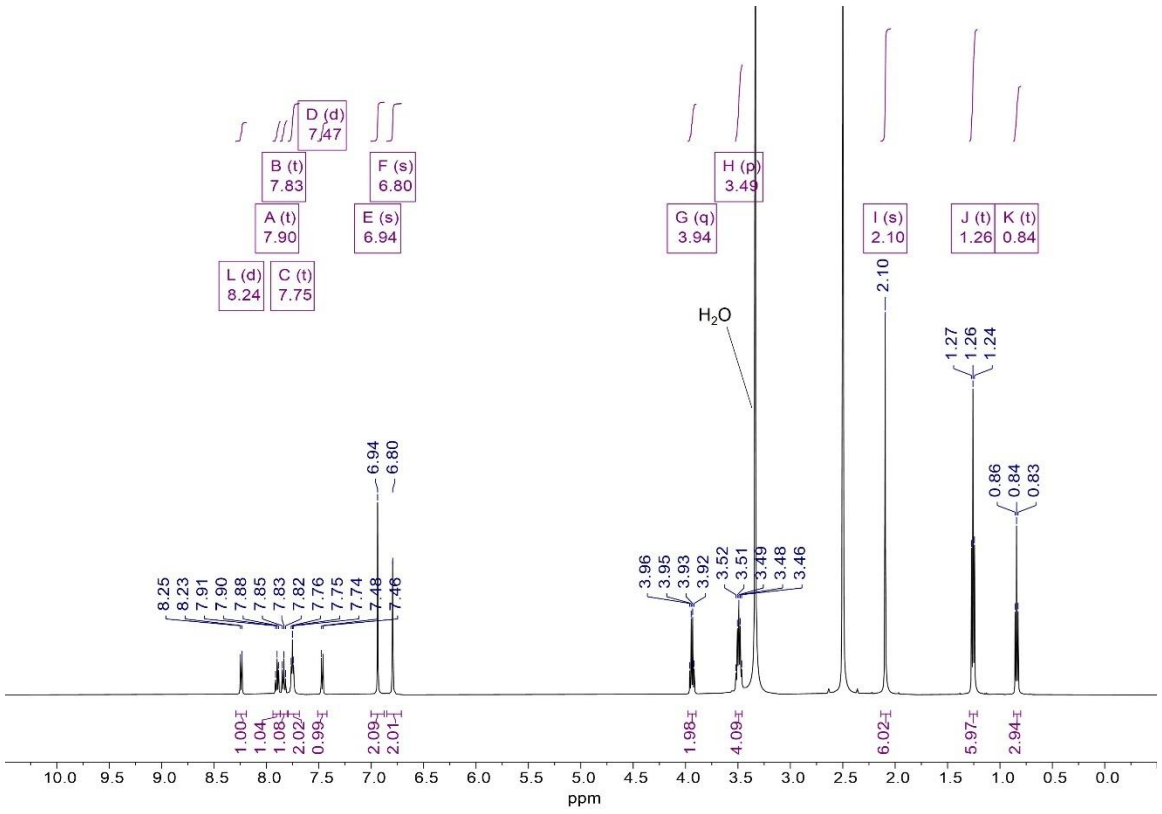

Figure S19. ^{1}H-NMR spectra of **R6g** in DMSO-d_6

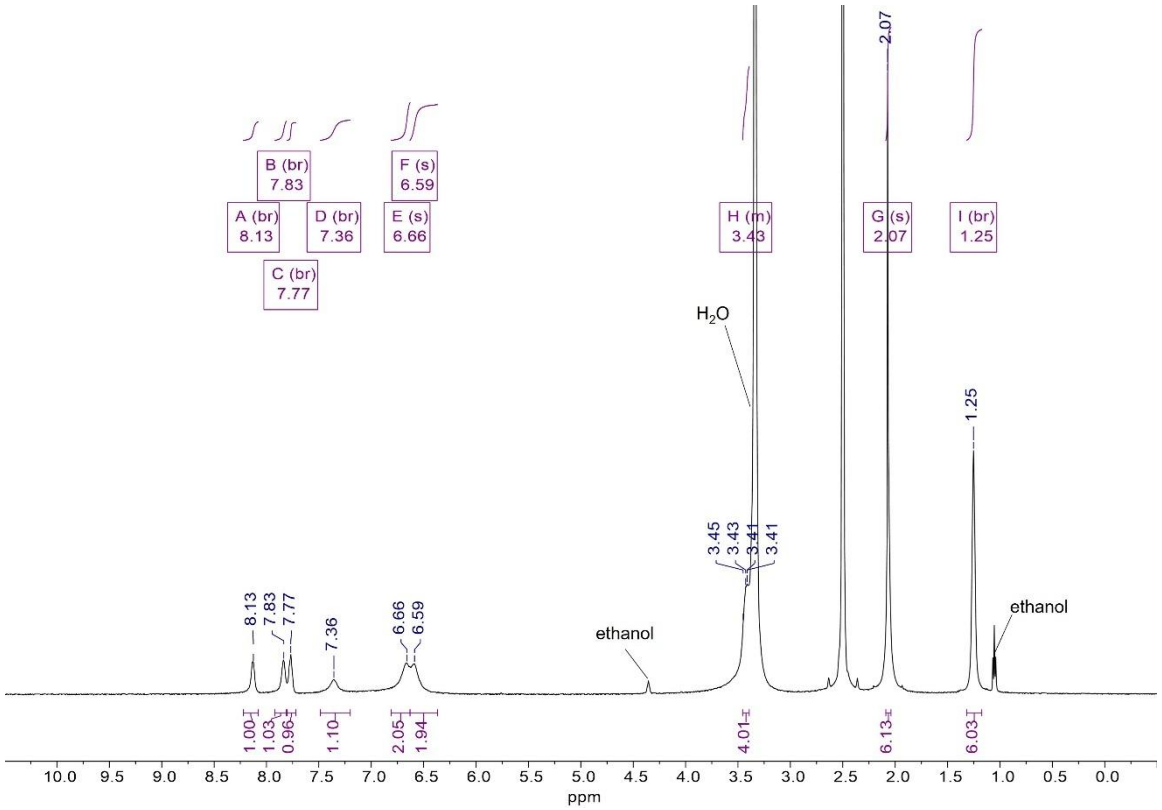

Figure S20. [1]H-NMR spectra of **Ni-1** in DMSO-d_6

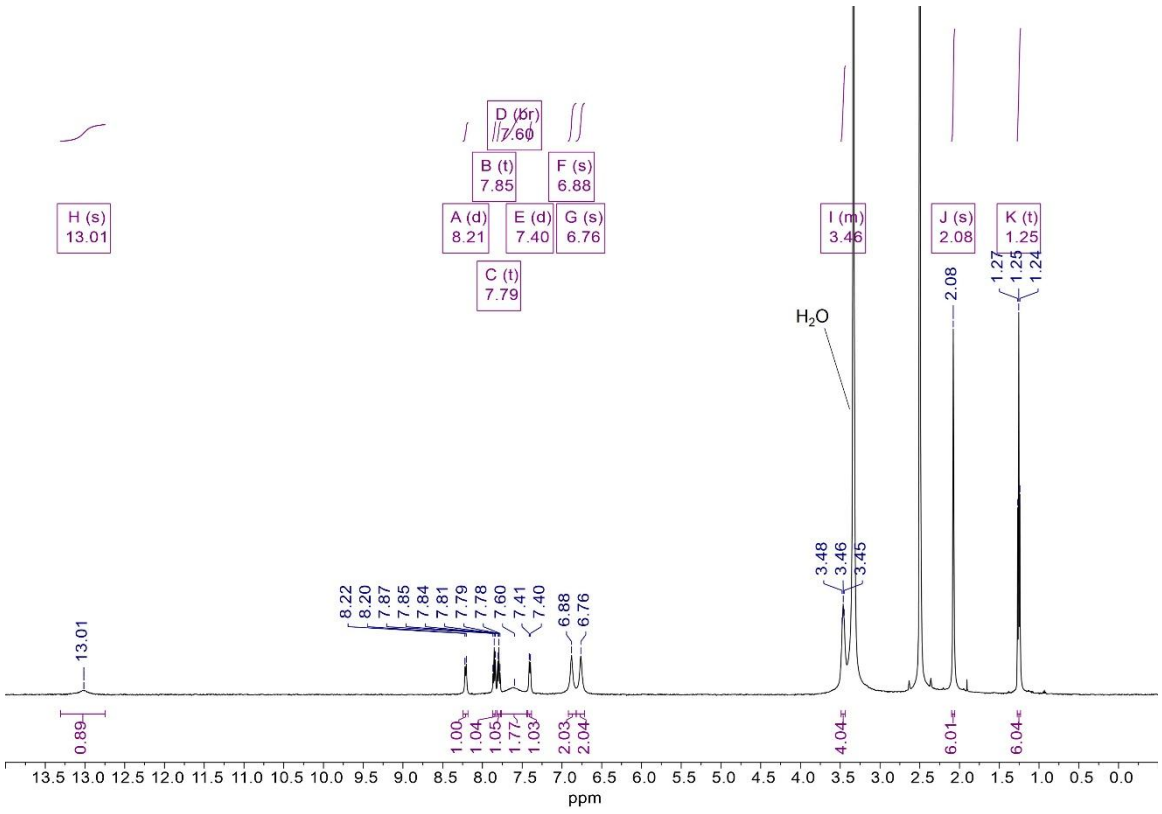

Figure S21. [1]H-NMR spectra of **Pd-1** in DMSO-d_6

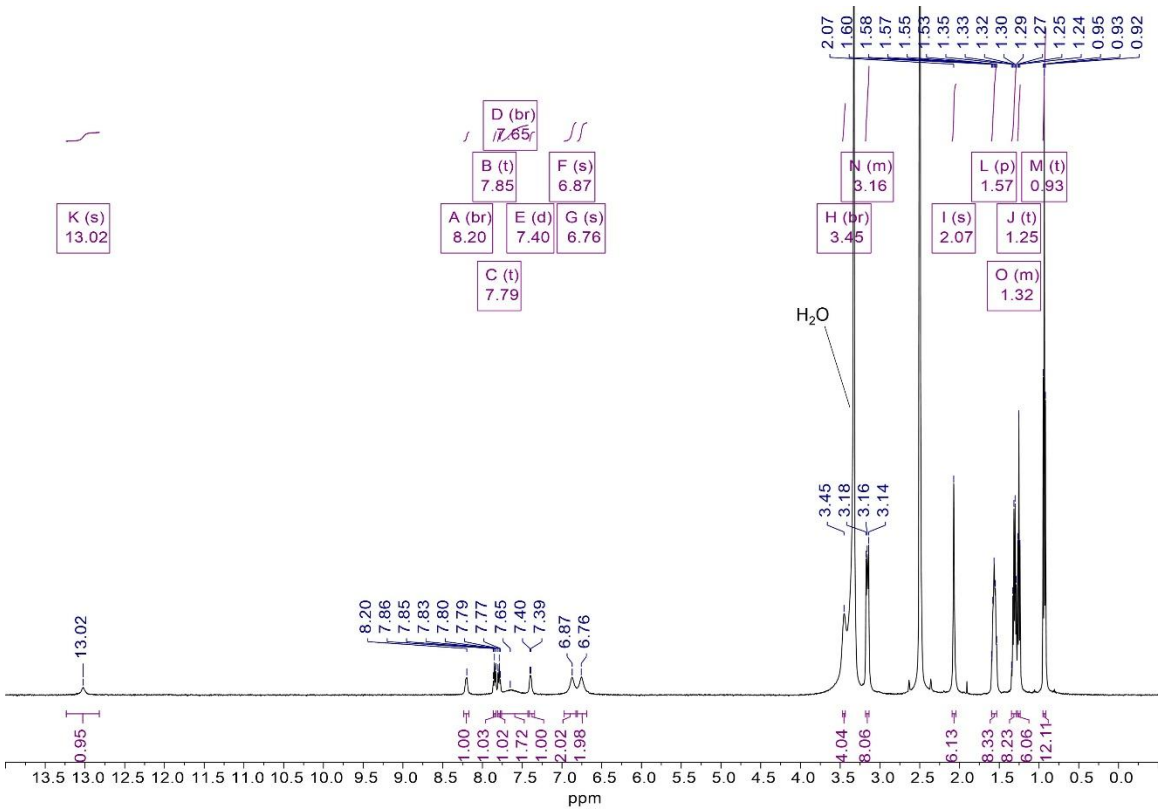

Figure S22. [1]H-NMR spectra of **Zn-1** in DMSO-d_6

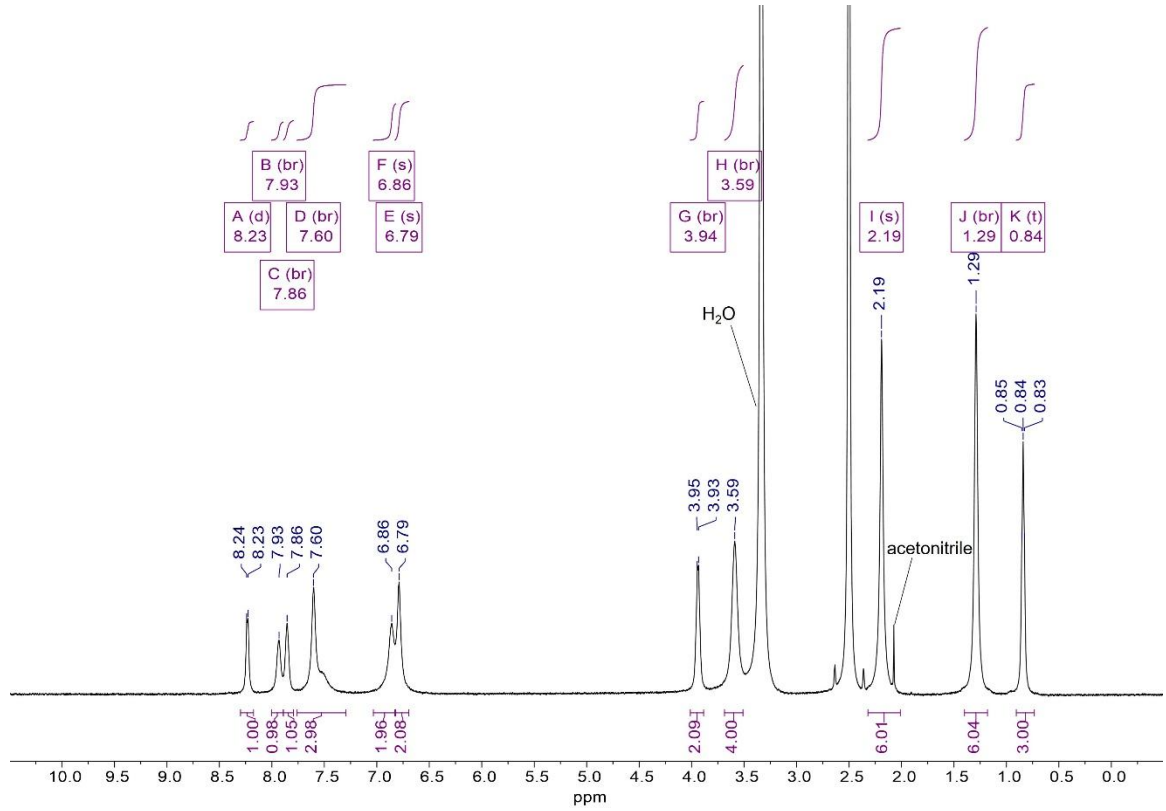

Figure S23. [1]H-NMR spectra of **Ni-2** in DMSO-d_6

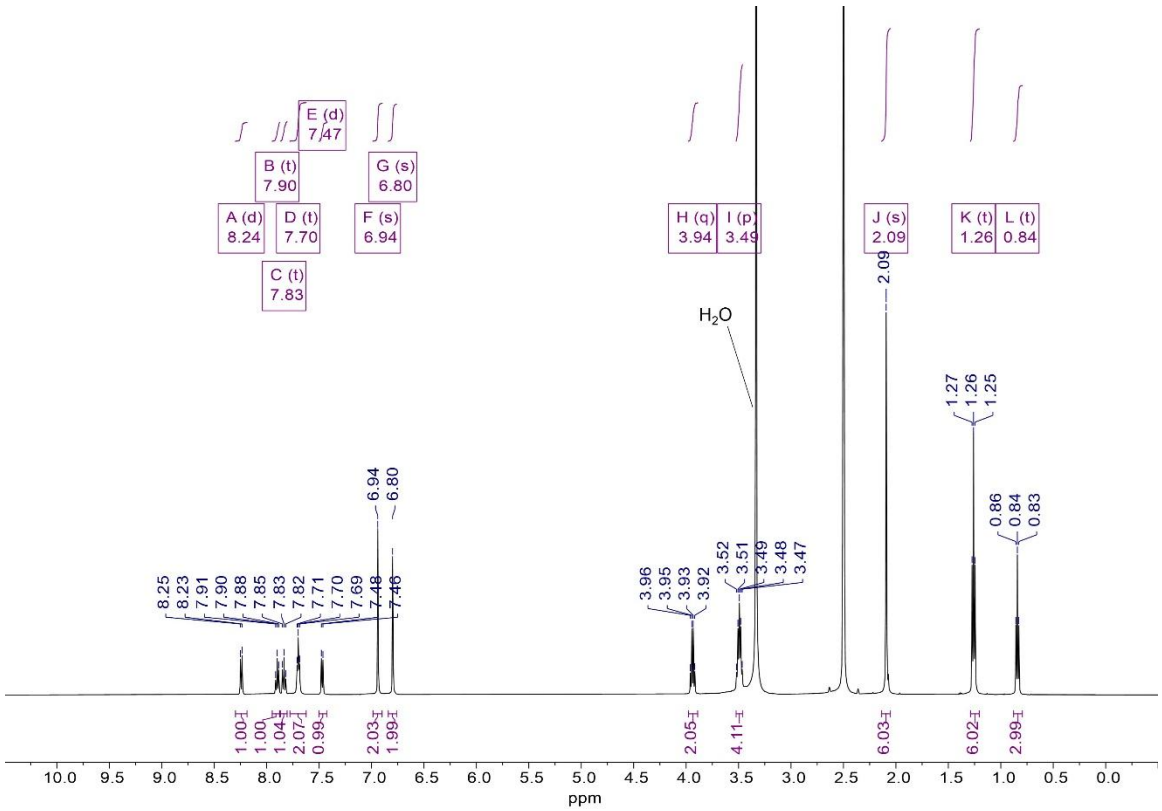

Figure S24. [1]H-NMR spectra of **Pd-2** in DMSO-d_6

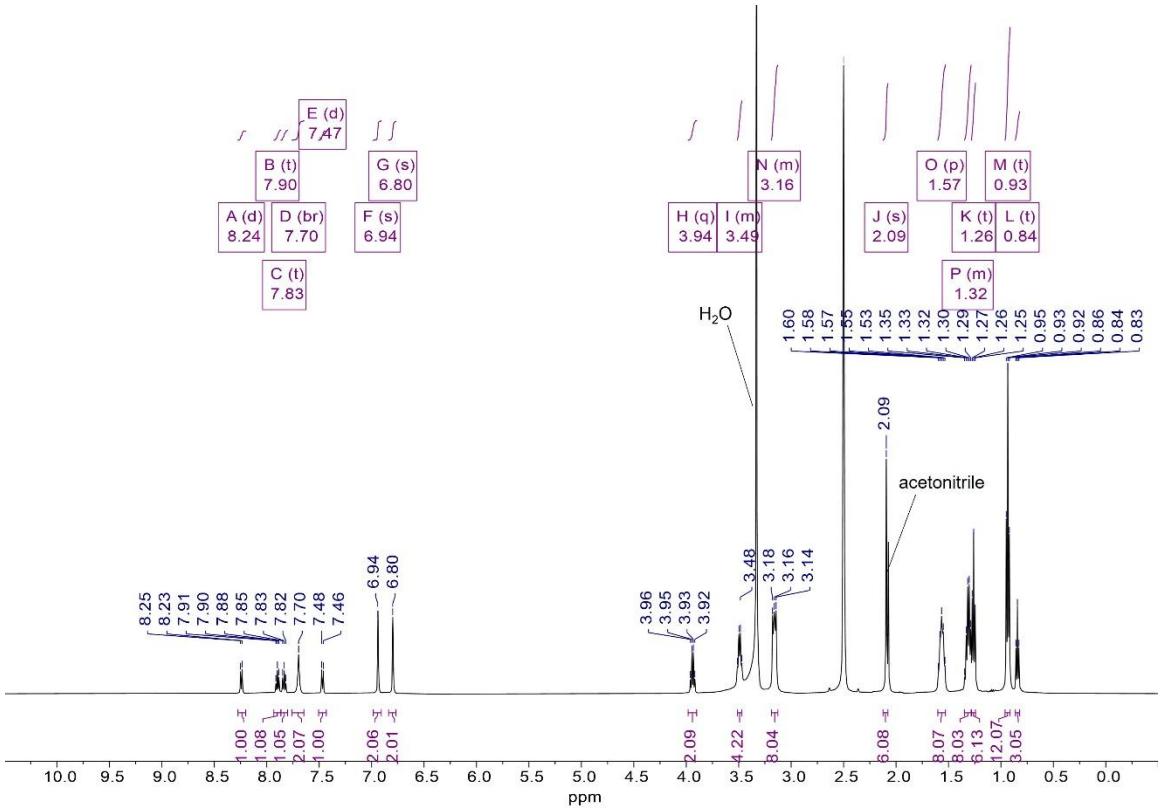

Figure S25. [1]H-NMR spectra of **Zn-2** in DMSO-d_6

7. Refinement Data of the X-ray Structures

Table S2. Crystal data and structure refinements for **Ni-1** (CCDC: 2479924) and **Ni-2** (CCDC: 2479921).

	Ni-1	**Ni-2**
Empirical formula	$C_{34}H_{33}N_2NiO_4S_{10}$	$C_{34}H_{31}N_2NiO_3S_{10}$
Formula weight	912.93	894.92
Temperature / K	296(2)	293(2)
Crystal system	Triclinic	Monoclinic
Space group	P-SS1	$P2_1/c$
a / Å	11.480(5)	28.6433(12)
b / Å	13.227(5)	11.3115(5)
c / Å	14.218(5)	15.862(3)
α / °	101.118(12)	90
β / °	97.148(13)	105.4380(10)
γ / °	98.529(14)	90
Volume / $Å^3$	2068.8(13)	7856.6(6)
Z	2	8
ρ_{calc} Mg/m^3	1.466	1.513
μ/mm^{-1}	1.012	1.063
F(000)	942	3688
Crystal size / mm^3	0.3x0.2x0.2	0.4×0.3×0.2
Radiation	MoKα (λ = 0.71073)	MoKα (λ = 0.71073)

2θ range for data collection/°	2.396 to 25.250	2.196 to 27.935
Index ranges	−13≤ h≤13, −15≤ k ≤15, −17≤ l ≤17	−37≤ h ≤37, −14≤ k ≤14, −33≤ l ≤30
Reflections collected	58888	113379
Independent reflections	7491 [R_{int} = 0.0590]	18803 [R(int) = 0.1122]
Data/restraints/parameters	7491/1/469	118803/0/911
Goodness-of-fit on F^2	1.040	1.046
Final R indexes [R>=2σ(I)]	R1 = 0.0434, wR2 = 0.1096	R1 = 0.0843, wR2 = 0.1471
Final R indexes [all data]	R1 = 0.0575, wR2 = 0.1179	R1 = 0.1565, wR2 = 0.1738
Largest diff. peak/hole / $eÅ^{-3}$	0.600/−0.397	1.583 / -0.930

Table S3. Crystal data and structure refinements for **Pd-1** (CCDC: 2479919) and **Pd-2** (CCDC: 2479923).

	Pd-1	**Pd-2**
Empirical formula	$C_{62}H_{60}N_6O_6PdS_{10}$	$C_{62}H_{58}N_4O_6PdS_{10}$
Formula weight	1412.16	1382.12
Temperature / K	304(2)	296(2)
Crystal system	Triclinic	Triclinic
Space group	P-1	P-1
a / Å	8.0052(2)	11.5454(17)
b / Å	12.2415(3)	12.1683(19)
c / Å	17.1514(5)	12.7456(19)
α / °	97.2910(10)	85.850(5)
β / °	103.4270(10)	64.210(5)
γ / °	90.2760(10)	88.366(5)

Volume / $Å^3$	1620.58(7)	1608.0(4)
Z	1	1
ρ_{calc} Mg/m^3	1.447	1.427
μ/mm^{-1}	0.663	0.666
F(000)	728	712
Crystal size / mm^3	0.4x0.3x0.2	0.5×0.4×0.3
Radiation	MoKα (λ = 0.71073)	MoKα (λ = 0.71073)
2θ range for data collection/°	2.463 to 28.018	2.363 to 27.956
Index ranges	−10≤ h≤10, −16≤ k ≤16, −22≤ l ≤22	−15≤ h ≤15, −16≤ k ≤16, −16≤ l ≤16
Reflections collected	47446	51298
Independent reflections	7793 [R_{int} = 0.0351]	7679 [R(int) = 0.0581]
Data/restraints/parameters	7793/0/417	7679/23/404
Goodness-of-fit on F^2	1.042	1.033
Final R indexes [R>=2σ(I)]	R1 = 0.0327, wR2 = 0.0892	R1 = 0.0440, wR2 = 0.1183
Final R indexes [all data]	R1 = 0.0396, wR2 = 0.0964	R1 = 0.0595, wR2 = 0.1306
Largest diff. peak/hole / $eÅ^{-3}$	0.375/−0.364	0.539 / -0.480

Table S4. Crystal data and structure refinements for **Zn-1** (CCDC: 2479926) and **Zn-2** (CCDC: 2479925).

	Zn-1	**Zn-2**
Empirical formula	$C_{48.25}H_{65}N_3O_{3.50}S_{10}Zn$	$C_{51}H_{69.25}N_3O_3S_{10}Zn$
Formula weight	1129.00	1158.31
Temperature / K	297(2)	296(2)

Crystal system	Triclinic	Triclinic
Space group	P-1	P-1
a / Å	11.5628(16)	13.410(3)
b / Å	13.435(2)	13.585(3)
c / Å	19.579(3)	19.962(4)
α / °	96.172(5)	97.868(7)
β / °	98.566(5)	101.818(7)
γ / °	90.161(5)	118.010(7)
Volume / $Å^3$	2989.7(8)	3026.1(11)
Z	2	2
ρ_{calc} Mg/m^3	1.254	1.271
μ/mm^{-1}	0.799	0.791
F(000)	1187	1220
Crystal size / mm^3	0.4x0.3x0.2	0.5×0.4×0.3
Radiation	MoKα (λ = 0.71073)	MoKα (λ = 0.71073)
2θ range for data collection/°	1.949 to 28.419	2.305 to 27.990
Index ranges	−15≤ h≤15, −17≤ k ≤17, −26≤ l ≤26	−17≤ h ≤17, −17≤ k ≤17, −26≤ l ≤26
Reflections collected	56093	139592
Independent reflections	14851 [R_{int} = 0.0968]	14536 [R(int) = 0.0482]
Data/restraints/parameters	14851/66/652	14536/27/661
Goodness-of-fit on F^2	1.032	1.091
Final R indexes [R>=2σ(I)]	R1 = 0.0810, wR2 = 0.2269	R1 = 0.0513, wR2 = 0.1498

Final R indexes [all data]	R1 = 0.1649, wR2 = 0.2898	R1 = 0.0631, wR2 = 0.1589
Largest diff. peak/hole / eÅ^{-3}	0.905/−0.621	0.985 / -0.420

8. IV Curves and Conductivities of M-1/2

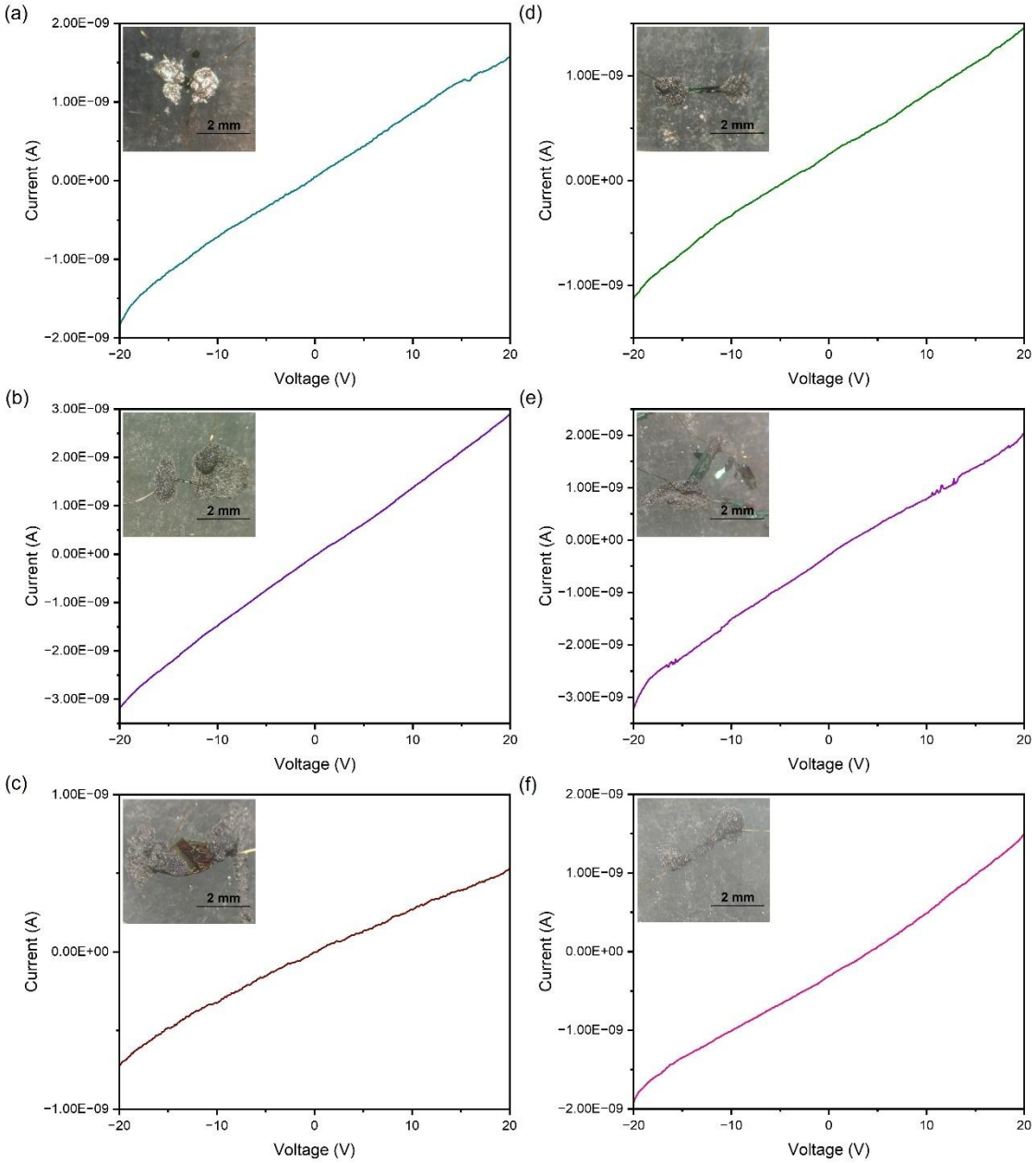

Figure S26. IV curves of **M-1/2**. Insets are corresponding fabricated devices. (a) **Ni-1** (b) **Pd-1** (c) **Zn-1** (d) **Ni-2** (e) **Pd-2** (f) **Zn-2.**

Conductivity was calculated according to Equation (3):

$$\sigma = \frac{1}{R}\frac{L}{A} \quad (3)$$

where R, L and A are resistance, length and area respectively.

Table S5. Conductivity of **M-1/2**

Single crystal	Conductivity(S/m)
Ni-1	$2.6X10^{-7}$
Pd-1	$9.3X10^{-6}$
Zn-1	$1.5X10^{-7}$
Ni-2	$1.2X10^{-6}$
Pd-2	$1.5X10^{-6}$
Zn-2	$7.8X10^{-7}$

References

1. Yilmaz M, Babur E, Ozdemir M, Gieseking RL, Dede Y, Tamer U*, et al.* Nanostructured organic semiconductor films for molecular detection with surface-enhanced Raman spectroscopy. *Nature Materials* 2017, **16**(9)**:** 918-924.
2. Zheng Z, Cong S, Gong W, Xuan J, Li G, Lu W*, et al.* Semiconductor SERS enhancement enabled by oxygen incorporation. *Nature Communications* 2017, **8**(1)**:** 1993.
3. Dennington, Roy, Keith, Todd A., Millam, John M., GaussView, Version 6, Semichem Inc., Shawnee Mission, KS, 2016.
4. Frisch, M. J., Trucks, G. W., Schlegel, H. B., Scuseria, G. E., Robb, M. A., Cheeseman, J. R., Scalmani, G., Barone, V., Petersson, G. A., Nakatsuji, H., et. al., Gaussian 16, Revision C.02, Gaussian, Inc., Wallingford CT, 2016.
5. Stephens PJ, Devlin FJ, Chabalowski CF, Frisch MJ. Ab Initio Calculation of Vibrational Absorption and Circular Dichroism Spectra Using Density Functional Force Fields. *The Journal of Physical Chemistry* 1994, **98**(45)**:** 11623-11627.
6. Grimme S, Antony J, Ehrlich S, Krieg H. A consistent and accurate ab initio parametrization of density functional dispersion correction (DFT-D) for the 94 elements H-Pu. *The Journal of Chemical Physics* 2010, **132**(15).
7. Grimme S, Ehrlich S, Goerigk L. Effect of the damping function in dispersion corrected density functional theory. *Journal of Computational Chemistry* 2011, **32**(7)**:** 1456-1465.

8. Hehre WJ, Ditchfield R, Pople JA. Self—Consistent Molecular Orbital Methods. XII. Further Extensions of Gaussian—Type Basis Sets for Use in Molecular Orbital Studies of Organic Molecules. *The Journal of Chemical Physics* 1972, **56**(5)**:** 2257-2261.

9. Hariharan PC, Pople JA. The influence of polarization functions on molecular orbital hydrogenation energies. *Theoretica chimica acta* 1973, **28**(3)**:** 213-222.

10. Igel-Mann G, Stoll H, Preuss H. Pseudopotentials for main group elements (IIIa through VIIa). *Molecular Physics* 1988, **65**(6)**:** 1321-1328.

11. Andrae D, Häußermann U, Dolg M, Stoll H, Preuss H. Energy-adjusted ab initio pseudopotentials for the second and third row transition elements. *Theoretica chimica acta* 1990, **77:** 123-141.

12. Scalmani G, Frisch MJ. Continuous surface charge polarizable continuum models of solvation. I. General formalism. *The Journal of Chemical Physics* 2010, **132**(11).

13. Lu T, Chen F. Multiwfn: A multifunctional wavefunction analyzer. *Journal of computational chemistry* 2012, **33**(5)**:** 580-592.

14. Lu T. A comprehensive electron wavefunction analysis toolbox for chemists, Multiwfn. *The Journal of Chemical Physics* 2024, **161**(8).

15. Liu Z, Lu T, Chen Q. An sp-hybridized all-carboatomic ring, cyclo[18]carbon: Electronic structure, electronic spectrum, and optical nonlinearity. *Carbon* 2020, **165:** 461-467.

16. Humphrey W, Dalke A, Schulten K. VMD: Visual molecular dynamics. *Journal of Molecular Graphics* 1996, **14**(1)**:** 33-38.